Investigation on Degradation Path of SF_6 in Packed-bed Plasma: Effect of Plasma-generated Radicals

Zhaolun Cui, *Member*, *CSEE*, Chang Zhou, Amin Jafarzadeh, Xiaoxing Zhang, *Member*, *CSEE*, Peng Gao, Licheng Li, *Member*, *CSEE*, and Yanpeng Hao, *Member*, *CSEE*

Abstract—SF_6 degradation mechanism in non-thermal plasma (NTP) systems is not fully understood due to the formation of a complex physico-chemical reaction network, especially when reactive gases and packing materials are involved. In this work, we conduct a combined experimental and theoretical study to unravel the SF_6 degradation path in a γ-Al_2O_3 packed plasma in the presence of H_2O or O_2. Our experimental results show that both H_2O and O_2 have a synergetic effect with γ-Al_2O_3 packing on promoting SF_6 degradation, leading to higher stable gas yields than typical spark or corona discharges. H_2O or O_2 addition promotes SO_2 or SO_2F_2 selectivity, respectively. Density functional theory (DFT) calculations reveal that SO_2 generation corresponding with the highest activation barrier is the most critical step toward SF_6 degradation. Radicals like H and O generated from H_2O or O_2 discharge can significantly promote the degradation process via Eley-Rideal mechanism, affecting key reactions of stable product generation, advancing degradation efficiency. The results of this work could provide insights on further understanding SF_6 degradation mechanism especially in packed-bed plasma systems.

Index Terms—Degradation mechanism, packed-bed plasma, radicals, SF_6.

I. INTRODUCTION

SULFUR hexafluoride (SF_6) is widely used as an insulation gas in power industry. However, SF_6 is a greenhouse gas with a global warming potential of 23,500 times that of CO_2 [1]. Meanwhile, SF_6 has a long lifetime of 3200 years in the atmosphere [2]. Emission of SF_6 caused by faults and retirements of gas-insulation equipment accounts for more than 80% of total emissions, accompanied by an annual growth of 20% [3], [4]. Usage and emission of SF_6 in power industry pose increasing threats to the environment.

In recent decades, various methods have been applied to treat SF_6 waste, such as thermal degradation, photocatalytic degradation, non-thermal plasma (NTP) treatment, and electrochemical degradation [5]. Among them, thermal degradation and NTP methods realized industrial applications. Thermal methods with $1100°C$ high-temperature conditions hold promise for large-scale degradation in power industry, but it suffers from low energy efficiency [6]. Since the early 20th century, NTP method has been applied to treat SF_6 waste at low concentrations (usually $< 1\%$) and small volumes in semiconductor industry [7]. However, due to the significant difference in SF_6 waste between power industry and semiconductor industry in terms of concentrations, impurity composition, content, and scale, to date, no commercial applications of NTP degradation in power industry have been reported.

One of the main issues that hinder NTP treatment of high-concentration SF_6 waste in power industry is the regulation of SF_6 decomposition path and its product selectivity [8]. Due to complexity of discharge and reactions, degradation path of SF_6 is difficult to be controlled, leading to an inevitable formation of toxic and corrosive gaseous products such as SO_2F_2, SOF_2, SOF_4, SO_2, S_2F_{10}, SF_4, and HF. Most acidic gases can be adsorbed by alkaline powers or their solutions, while SO_2F_2 and SOF_4 are insoluble in water and react slowly with alkaline materials, which significantly hinder the recovery of tail gases [9]. In this regard, researchers found addition of reactive gases such as H_2, H_2O, NH_3 can react with SF_6, as well as its primary decompositions, thus regulating SF_6 degradation path and reducing yield of oxyfluoride (S-O-F) products [10], [11]. Similarly, packing solid materials like γ-Al_2O_3 can affect reactions and product properties by changing discharge parameters and providing gas-solid interface reactions [12]. However, the above studies focused mainly on the experimental level, and the detailed reaction mechanism of SF_6 degradation in plasma region is still unknown, especially for packed bed plasma systems.

So far, reaction analysis of SF_6 plasma degradation is usually referred to as the SF_6 decomposition mechanism in electrical equipment [13]. In gas-insulated equipment like gas-insulated switchgear (GIS) and gas-insulated line (GIL), insulation faults such as partial discharges, partial over-thermal fault, and electrodes breakdown cause decomposition of SF_6 to SF_x ($x < 6$) and F. Then SF_6 and SF_x can react with trace

amounts of O_2 and H_2O to generate products like SO_2F_2, SOF_2, SOF_4, SO_2, H_2S [14], [15]. Although decomposition reactions and products of SF_6 in power equipment is quite similar to SF_6 degradation in NTP treatment, there are still some clear differences. First, SF_6 decomposition reactions in power equipment mostly happen in gas phase, and the amount of SF_6 decomposition is very limited (much less than 1%). But in a NTP treatment, especially in a packed-bed plasma, gas-solid interface could be the most important reaction area which differs significantly from gas phase. Besides, effects of radicals are usually not considered in SF_6 decomposition studies, but are very important in plasma-induced reactions [16]. In a word, directly applying the SF_6 decomposition mechanism to NTP degradation is arbitrary, especially when reactive gases and packing materials are considered. The unknown degradation mechanism of SF_6 in the NTP treatment hinders the determination of degradation conditions to achieve high energy efficiency and desirable products, which needs comprehensive investigation.

To unravel the degradation mechanism of SF_6 to stable products in the NTP system, we take γ-Al_2O_3 packed-bed dielectric barrier discharge (PB-DBD) as a typical NTP approach with H_2O or O_2 additions. Our previous study has proved γ-Al_2O_3 packing in DBD plasma can promote degradation efficiency and regulate product selectivity [12]. In this work, combined effects of γ-Al_2O_3 packing and reactive gas addition (H_2O, O_2) on SF_6 degradation efficiency and product selectivity are experimentally investigated. Adsorption properties of main SF_6 decompositions, possible degradation paths, and the effect of plasma-generated radicals are studied via density functional theory (DFT). This study proves plasma radicals significantly improve surface reactions, and a detailed description on SF_6 degradation process is given for a better understanding of the decomposition mechanism in a PB-DBD system.

II. METHOD

A. Experimental Set-up

Details of the experimental setup can be referred to in our previous study [17], and the schematic diagram is shown in Fig. 1. γ-Al_2O_3 pellet with a 4 mm diameter is chosen as packing material in the DBD reactor. It's kept dry before packing and it undergoes a pre-discharge in Ar atmosphere before SF_6 degradation treatment. Since the high concentration of SF_6 significantly reduces discharge, the initial concentration of SF_6 is kept at 3% with 97% Ar as background gas. Flowrate is controlled at 150 mL/min. H_2O and O_2 are considered as reactive gases with concentration ranges of 0.25%–2.5% and 0.05%–4%, respectively. After degradation, three main stable products, i.e., SOF_2, SO_2F_2, and SO_2 are detected by a gas chromatography-mass spectrometry (GCMS, Shimadzu QP2020-NX), which has a detection limit to be 1 ppm (part per million, volume fraction) level.

The degradation removal efficiency E_{DRE} is calculated by:

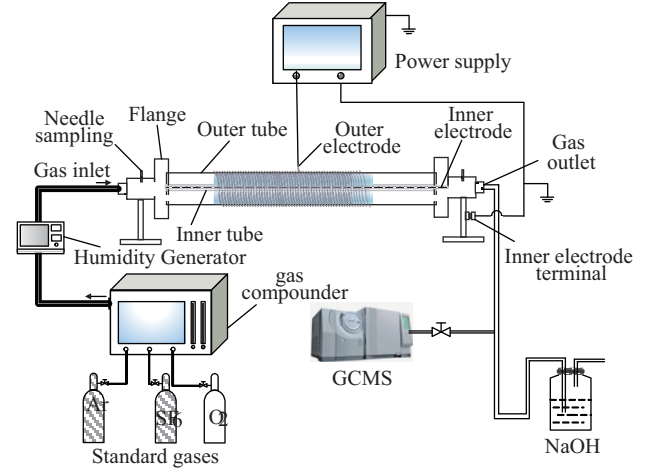$$E_{DRE} = \frac{C_i - C_f}{C_i} \times 100\% \tag{1}$$

Fig. 1. Schematic diagram of the experiment set-up.

where C_i and C_f mean initial and final concentrations of SF_6, respectively.

In tail gas, SOF_2, SO_2F_2, and SO_2 are detected, and their selectivity S_x are calculated by:

$$S_x = \frac{C_x}{C_{sum}} \times 100\% \tag{2}$$

where C_x and C_{sum} are concentrations of product x and initial concentration of SF_6 (3%).

Formation rate F_x of three products in this paper are calculated by:

$$F_x = \frac{Y_x}{P_i} \tag{3}$$

where Y_x is yield coefficient of product x, with a unit of nmol/s; P_i is input power, with a unit of J/s; Unit of F_x is nmol/J.

B. Computational Details

Computational work is carried out in CP2K 7.0 package by the Quickstep module [18]. Gaussian and plane wave method (GWP) is applied with double-ζ valence plus polarization (m-DZVP) basis set [19]. The cutoff set for plane wave calculation is 600 Ry. Electron exchange and correlation terms in the Kohn-Sham equation are described by the Perdew-Burke-Ernzerhof functional [20]. Grimme's D3 method is used to treat dispersion correction [21]. We consider 6, 7, 3, 6, and 1 valence electrons for S, F, Al, O, and H elements as their upper shell electrons, respectively. Inner shell electrons are approximately treated by the Goedecker-Teter-Hutter pseudopotentials [22]. Broyden-Fletcher-Goldfarb-Shanno scheme is used for geometry optimization [23]. Climbing-image nudged elastic band (CI-NEB) method is applied for transition state calculations [24]. k-point sampling is kept to Γ-point only.

A four-layer γ-Al_2O_3 (110) slab is built to represent γ-Al_2O_3 active surface [25], with an XYZ size of 16.1439 $\times$ 16.7874 $\times$ 40.0000 Å³, as shown in Fig. 2. More details about the slab modeling have been introduced in our previous study [17]. Al_{III} site over γ-Al_2O_3 (110) surface is selected as the active site for adsorption and reaction [26], as labelled in Fig. 2. During calculation, the bottom two layers of the
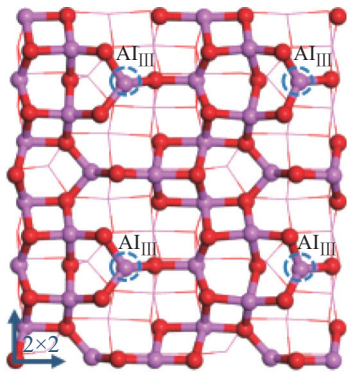
Fig. 2. Perfect 2×2 γ-Al$_2$O$_3$ (110) slab model and Al$_{III}$ surface site. Red and pink balls are O and Al atoms, respectively.

γ-Al$_2$O$_3$ (110) slab are fixed. After geometry optimization, adsorption energy E_{ad} can be calculated by:

$$E_{ad} = E_{gas+slab} - E_{gas} - E_{slab} \tag{4}$$

where E_{gas}, E_{slab} and $E_{gas+slab}$ are energies of gas molecules, slab, and gas-adsorbed system, respectively.

III. RESULTS AND DISCUSSION

A. Degradation Product Distributions in The γ-Al$_2$O$_3$ Packed DBD with H$_2$O or O$_2$ Additions

Distributions of degradation removal efficiency (E_{DRE}) and selectivity of three main products as a function of H$_2$O or O$_2$ concentrations are shown in Fig. 3. The upper and lower figures are the top views and the side views. Red, pink, yellow, cyan and white are O, Al, S, F and H atoms, respectively. Optimal concentrations of H$_2$O and O$_2$ for SF$_6$ degradation are found to be 0.5% and 0.1%, respectively. In Fig. 3(a), the highest yields of SO$_2$F$_2$, SOF$_2$, and SO$_2$ are 11636 ppm (0.25% H$_2$O), 1009 ppm (0.5% H$_2$O), and 7958 ppm (2.5% H$_2$O), respectively. Selectivity of SO$_2$F$_2$ decreases with H$_2$O concentration increasing, from 49.78% at 0.25% H$_2$O to 26.76% at 2.5% H$_2$O. On the contrary, SO$_2$ selectivity increases from 14.50% to 42.97%. SOF$_2$ selectivity increases from 1.81% at 0.25% H$_2$O to 4.06% at 0.5% H$_2$O, and then remains stable at around 4% with H$_2$O concentration increasing. In Fig. 3(b), the highest yields of SO$_2$F$_2$, SOF$_2$, and SO$_2$ are 9326 ppm (1% O$_2$), 176 ppm (1% O$_2$), and 6809 ppm (0.05% O$_2$), respectively. Increasing O$_2$ promotes SO$_2$F$_2$ selectivity from 31.23% at 0.05% O$_2$ to 53.08% at 4% O$_2$, while SO$_2$ selectivity is reduced from 33.27% to 10.95%. In the meantime, SOF$_2$ selectivity is kept below 1% at all O$_2$ concentrations. In general, the addition of H$_2$O significantly improves the generation of SO$_2$ and suppresses SO$_2$F$_2$, while O$_2$ addition leads to higher SO$_2$F$_2$ yields. These phenomena also show up in non-packed NTP systems and other packed-bed DBD systems [10], [27]–[29], which proves a regulation property of reactive gases on SF$_6$ degradation products. In this system, the sum of three stable products (SO$_2$F$_2$, SOF$_2$, and SO$_2$) accounts for 60%–75% of the total degradation of S products. The other products could be some primitive decompositions or relatively unstable products like SF$_4$, S$_2$F$_{10}$, SOF$_4$ and SO$_2$F, which has been investigated by the Fourier
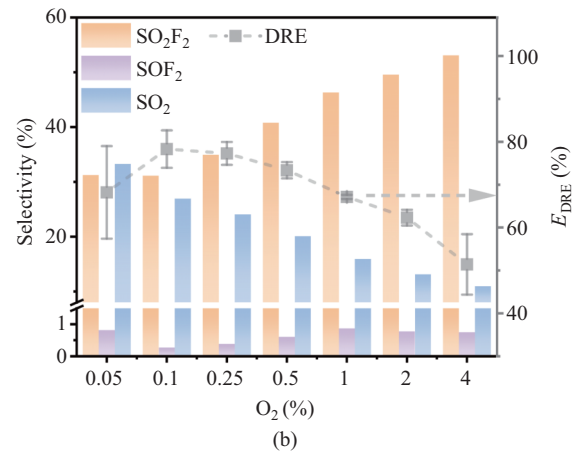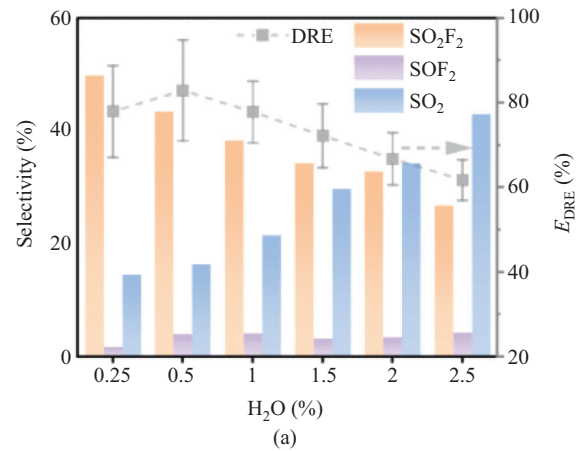

Fig. 3. The degradation removal efficiency E_{DRE} and the product selectivity upon H$_2$O or O$_2$ addition (3%SF$_6$-97%Ar, 80 W, 150 mL/min, 4 mm γ-Al$_2$O$_3$ packing). (a) H$_2$O (%). (b) O$_2$ (%).

transform infrared spectroscopy in previous studies [5], [11], [26].

Compared to SF$_6$/Ar degradation in γ-Al$_2$O$_3$ packed DBD [12], the total amount of three stable products (SO$_2$F$_2$, SOF$_2$, and SO$_2$) account for only about 40% in the SF$_6$/Ar system at 80 W, but increases to about 70% when proper concentrations of H$_2$O or O$_2$ are added (this study). This indicates that the addition of reactive gases has a synergetic effect on the packing material (γ-Al$_2$O$_3$), which jointly improves the sufficiency of SF$_6$ degradation. Besides, in a non-packed system with relatively sufficient degradation of SF$_6$, SOF$_4$ yields the highest tail gas, no matter H$_2$O or O$_2$ additions [30]. However, in the packing system, SO$_2$ and SO$_2$F$_2$ gradually show the highest selectivity in H$_2$O or O$_2$-rich systems, respectively (Fig. 3). This indicates SOF$_4$ is relatively unstable in the packing system and can undergo further decomposition to generate both SOF$_2$ and SO$_2$, affected by additions of different reactive gases. The underlying reactions are discussed in detail in Sections III-C and III-D.

To further evaluate the generation properties of three gas products in PB-DBD, we made a comparison of product yields in this work and in three typical gas-insulation faults, as shown in Table I [31]. In arc fault, SF$_6$ decomposes rapidly, and SOF$_2$ is the only stable product which shows a formation rate of 600 nmol/J in the Al electrode system and 50–150

TABLE I
YIELDS OF SF$_6$ BY-PRODUCTS FORMATION AT THREE TYPICAL GAS-INSULATION FAULTS AND IN THE PB-DBD SYSTEM

Discharge type	Work condition	Discharge characters	Formation rate (nmol/J)
Arc		3–100 kA, 50–150 ms, 10^5–10^7 J	SOF$_2$: 600 (Al electrode) 50–150 (Cu electrode)
Spark	Up to 99.9% SF$_6$ 0.1%–1% Air 100–500 ppm H$_2$O 100–500 ppm CF$_4$ 0.2–0.6 Mpa	μs duration, 10^{-1}–10^2 J/spark	SOF$_2$: 0.9–2.7 SOF$_4$: 0.13–0.31 SO$_2$F$_2$: 0.006–0.026 SO$_2$: 0.005
Corona & partial discharge		10–10^5 pC 10^{-3}–10^{-2} J/pulse 10^2–10^4 Hz	SOF$_2$: 1.3–5.2 SO$_2$F$_2$: 1.3–4.5 SOF$_4$: 5.8–8.6
PB-DBD (This work)	0.5% H$_2$O	10 kHz, 20–50 mA, 40–60 W	SO$_2$F$_2$: 16.0–26.7 SOF$_2$: 1.1–2.5 SO$_2$: 8.7–25.6
	0.25% O$_2$		SO$_2$F$_2$: 19.5–33.3 SOF$_2$: 0.17–0.55 SO$_2$: 6.9–20.9

nmol/J in the Cu electrode system [32], [33]. Intense discharge accompanied by high-temperature generation (up to 3000–12000°C) in the arc region accounts for SF$_6$ decomposition, and SOF$_2$ is generated from further reactions via SF$_4$ and SF$_2$ [31], [34]. By contrast, distributions of products are scattered, and yields are significantly lower in either spark fault or corona (partial discharge) fault, which is mainly attributed to their low energy density. Besides, even though the gas temperature in the spark (500–6000°C) is much higher than in the corona (200–1000°C) [35], the formation rate in the spark is much lower. It may be caused by high instantaneous current and short duration of spark. Thus, recombination of SF$_6$ happens immediately after discharge, and deep decomposition is reduced. In PB-DBD treatment of this work, formation rates of SO$_2$F$_2$ and SO$_2$ are larger in order of magnitude than in the corona fault. Electric field enhancement by packing materials and plasma-catalysis effects account for better performance in PB-DBD systems [36]. However, the formation rate in PB-DBD is still lower than in arc fault, especially for Al electrode system. There could be two main reasons. The first one is significantly lower energy density of PB-DBD system. The other is high temperature of arc system, which promotes rapid thermal-decomposition of SF$_6$ and increases rate of key reactions [37]. In general, we can achieve a relatively high yield of stable products via PB-DBD treatment at relatively energy-saving conditions, which shows a potential for portable or integrated industrial applications.

B. Adsorption Properties of SF$_6$ Decompositions Over The γ-Al$_2$O$_3$ (110) Surface

To determine possible elementary reactions of SF$_6$ degradation over gas-solid interface, we first calculated adsorption properties of SF$_6$ 16 main decompositions over γ-Al$_2$O$_3$ (110) surface. Adsorption configurations are shown in Fig. 4, adsorption energy E_{ad} and bonding properties are summarized in Table II. Before adsorption, each gas molecule has been optimized in gas phase and then is placed at Al$_{III}$ site as initial configuration.

As shown in Table II, adsorption results for these decomposition products vary greatly, with some being stable and bonded at the active site, some undergoing only physical adsorption, and some being unstable and undergoing further

TABLE II
ADSORPTION RESULTS FOR MAIN DECOMPOSITION PRODUCTS

Species	E_{ad} (eV)	Status
SF$_5$	−2.15	Bonded with the Al$_{III}$ atom
S$_2$F$_{10}$	−0.71	Decomposed to SF$_4$, SF$_5$ and F*
SF$_5$OH	−0.98	Bonded with the Al$_{III}$ atom
SOF$_5$	−2.35	Bonded with the Al$_{III}$ atom
SOF$_4$	−0.74	Bonded with the Al$_{III}$ atom
SF$_4$	−0.31	Physical adsorption
SF$_4$OH	−0.67	Bonded with the Al$_{III}$ atom
SF$_3$OH	−2.17	Decomposed to SOF$_2$* and HF*
SO$_2$F$_2$	−0.74	Bonded with two surface Al atoms
SOF$_3$	−2.90	Decomposed to SOF$_2$* and F*
SOF$_2$	−0.93	Bonded with the Al$_{III}$ atom
SO$_2$F	−2.00	Bonded with two surface Al atoms
SO$_2$	−1.50	Bonded with surface Al and O atoms
SOF	−1.21	Decomposed to SO* and F*
SO	−2.40	Bonded with surface Al and O atoms
HF	−2.54	Decomposed to H* and F*

*means the molecule is in adsorption state and bonded with γ-Al$_2$O$_3$ surface atoms

decomposition. First, SF$_5$, SF$_5$OH, SOF$_5$, SOF$_4$, SF$_4$OH, and SOF$_2$ can bond with atom Al$_{III}$, with E_{ad} of −2.15 eV, −0.98 eV, −2.35 eV, −0.74 eV, −0.67 eV, and −0.93 eV, respectively, indicating these six molecules are relatively stable and undergo chemisorption processes at the active site. Second, SO$_2$F$_2$, SO$_2$F, SO$_2$ and SO can bond to surface O or other surface Al in addition to Al$_{III}$ atoms with E_{ad} of −0.74 eV, −2.00 eV, −1.50 eV, and −2.40 eV, respectively, which also shows strong stability. Third, SF$_4$ molecules show physical adsorption above Al$_{III}$ site without bonding and have an E_{ad} of −0.31 eV. Finally, the remaining molecules are unstable. After geometry optimization, S$_2$F$_{10}$ decomposes to SF$_4$, SF$_5$, and F* (* indicates particles are in theadsorbed state). SF$_3$OH decomposes into SOF$_2$* and HF*. SOF$_3$ decomposes into SOF$_2$* and F* atoms. SOF decomposes into SO* and F*. HF decomposes into H* and F*. The above results indicate the five molecules are likely to further decompose, forming new decomposition products on γ-Al$_2$O$_3$ surface.

C. Degradation Reactions of SF$_6$ Over The γ-Al$_2$O$_3$ (110) Surface

Referring to relevant study of SF$_6$ decomposition paths [13]–[15], [38], as well as experimental results in this work,
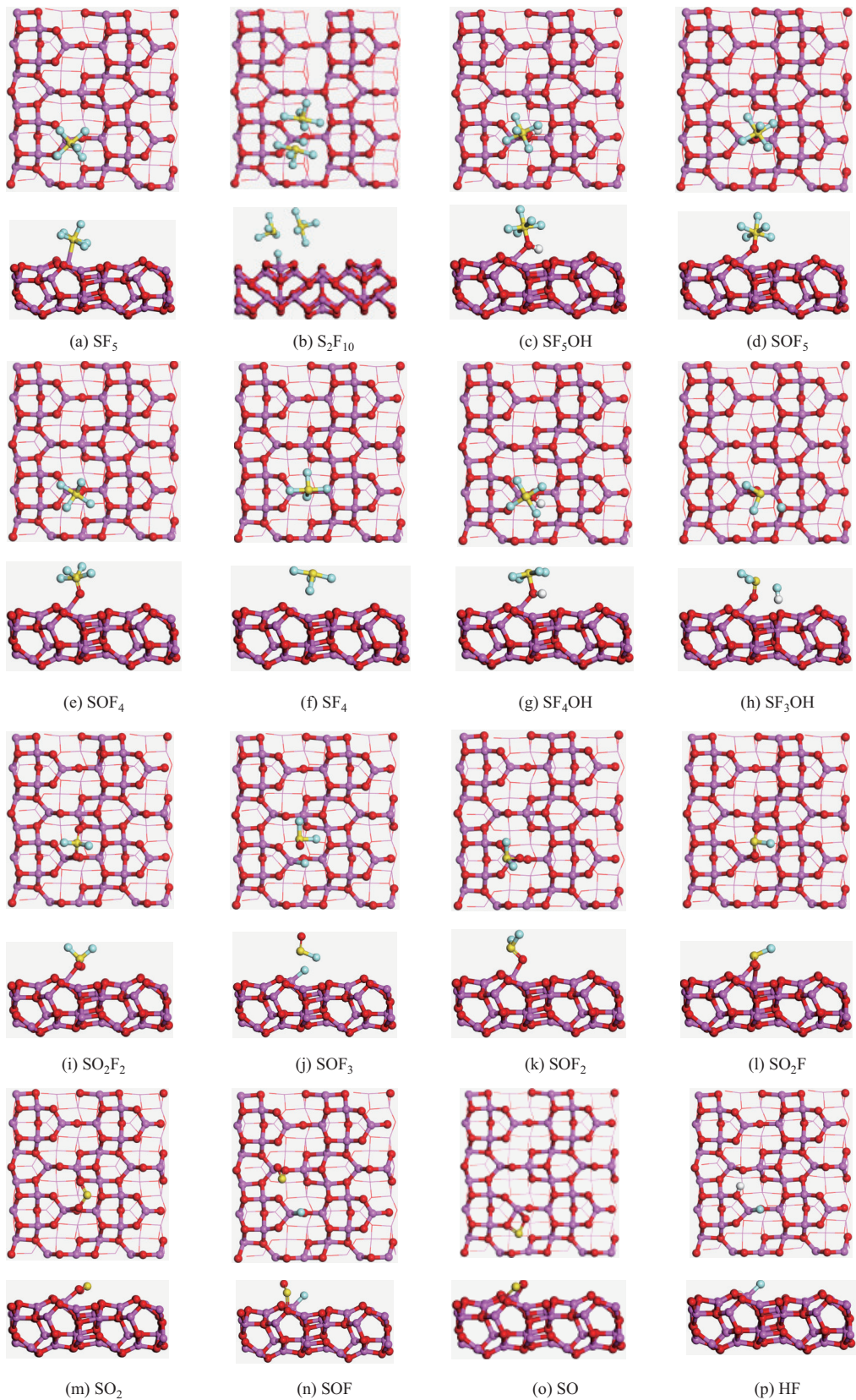
Fig. 4. Adsorption configurations of SF$_6$ decompositions at the Al$_{III}$ site over the γ-Al$_2$O$_3$ (110) surface. The upper and lower figures are the top views and the side views. Red, pink, yellow, cyan and white are O, Al, S, F and H atoms, respectively.

potential decomposition path of SF_6 over γ-Al_2O_3 (110) surface is speculated and elementary reactions are calculated, as shown in Fig. 5. The number of equations and their corresponding activation barrier are labelled near the arrows. The ΔE mentioned in gas phase reaction (4) means the reaction heat. The '(g)' and the '*' after the molecular formula mean the gas state and the adsorption state, respectively. Yellow labelled are unstable products or intermediates, which themselves easily decompose over γ-Al_2O_3 surface. SO_2 is labelled as a desired product in green as it is a main product and can be easily handled by an alkaline solution. Activation barrier and reaction heat for elementary reactions are summarized in Table III. Yellow intermediates could also be predecessors of some key decomposition products. Therefore, in calculation of elementary reactions, we only calculated reactions of these unstable molecules as reactants, while their formation reactions are difficult to be calculated by NEB

Fig. 5.   The possible decomposition pathway of SF_6 via LH mechanism in the γ-Al_2O_3 packed system.

TABLE III
ACTIVATION BARRIER E_a AND REACTION HEAT ΔE FOR ELEMENTARY
REACTIONS OF SF_6 DEGRADATION OVER THE γ-Al_2O_3 (110) SURFACE

No.	Reaction	E_a (eV)	ΔE (eV)
(5)	$SF_6(g) \rightarrow SF_5(g) + F(g)$	–	4.20 [39]
(6)	$SF_6^* \rightarrow SF_5^* + F^*$	1.80 [14]	−1.29 [14]
(7)	$SF_5^* \rightarrow SF_4^* + F^*$	0.01	−1.98
(8)	$SF_5^* + OH^* \rightarrow SF_5OH^*$	0.00	−1.61
(9)	$SF_5OH^* \rightarrow SOF_5^* + H^*$	0.00	−0.64
(10)	$SOF_5^* + H^* \rightarrow SOF_4^* + HF^*$	0.77	0.39
(11)	$SF_4^* + O^* \rightarrow SOF_4^*$	0.50	−1.27
(12)	$SF_4^* + OH^* \rightarrow SF_4OH^*$	1.12	0.70
(13)	$SOF_3^* \rightarrow SOF_2^* + F^*$	0.00	−1.22
(14)	$SF_3OH^* \rightarrow SOF_2^* + HF^*$	0.00	−1.62
(15)	$SOF_2^* + O^* \rightarrow SO_2F_2^*$	0.79	−1.97
(16)	$SOF^* \rightarrow SO^* + F^*$	0.00	−0.62
(17)	$SO^* + O^* \rightarrow SO_2^*$	0.00	−4.28
(18)	$SO_2F_2^* \rightarrow SO_2F^* + F^*$	2.57	0.78
(19)	$SO_2F^* \rightarrow SO_2^* + F^*$	2.63	−0.68
(20)	$H^* + F^* \rightarrow HF(g)$	1.17	1.11
(21)	$SF_4^* + O(g) \rightarrow SOF_4^*$	0.00	–
(22)	$SOF_2^* + O(g) \rightarrow SO_2F_2^*$	0.00	–
(23)	$H(g) + SO_2F \rightarrow SO_2^* + H^* + F^*$	0.00	–
(24)	$H(g) + SOF_4^* \rightarrow SOF_3^* + HF(g)$	0.00	–
(25)	$H(g) + F^* \rightarrow HF(g)$	0.00	–
(26)	$H^* + F(g) \rightarrow HF(g)$	0.00	–

(g) means the molecule is initialed in the gas phase. * means the adsorption state.

methods.

As shown in Fig. 5, adsorbed SF_6^* first decomposes to SF_5^* and F^* on γ-Al_2O_3 surface by initial bond breaking, with an energy barrier of 1.80 eV [17]. Then SF_5^* can further break the S-F bond to form SF_4^* and F^* by reaction (7) with a reaction energy barrier of 0.01 eV and reaction heat of −1.98 eV. Besides, SF_5^* can react with OH^* to form SF_5OH^* by reaction (8), which is an exothermic reaction with reaction heat of −1.61 eV and has no obvious barrier. In other words, although SF_5^* can be adsorbed at active site, but the structure is not stable, and it can easily react with other species or decompose to form more stable products.

Then SF_5OH^* can gradually leave H and F atoms to produce stable product SOF_4^* by reaction (9) and (10). The reaction (9) has no obvious energy barrier and is exothermic. In reaction (10), F atoms in the SOF_5 molecule combine with adsorbed H^* atoms on the surface and detach from SOF_5^* with an energy barrier of 0.77 eV. Alternatively, SOF_4^* can also be produced by reaction (11) where SF_4^* combines with O^* atoms, having a reaction energy barrier of 0.50 eV. Moreover, SF_4^* can bond with OH^* to produce SF_4OH^* via reaction (12), which has an energy barrier of 1.12 eV. Afterwards, SOF_4^* and SF_4OH^* could decompose to produce unstable intermediates like SOF_3^* and SF_3OH^*, and then these two unstable species undergo further decompositions to generate SOF_2^* via reactions (13) and (14) without any activation barrier.

Next, SOF_2^* can be bonded to O^* to produce $SO_2F_2^*$ via reaction (15), or alternatively loses one F atom to produce SOF^* molecules. Due to instability of SOF^*, it may decompose to SO^* and F^* atoms via reaction (16), while SO^* can react with adsorbed O^* atoms to produce SO_2^* by reaction (17). Our results and related studies suggest SO_2F may be an important intermediate [15], [40]. It can be generated from SO_2F_2 decomposition via reaction (18), with a high energy barrier of 2.57 eV. Then SO_2F^* can undergo further decomposition to generate SO_2^* and F^* via reaction (19) ($E_a = 2.63$ eV). These two reactions are rate-limiting steps of SF_6 degradation via LH mechanism in the already calculated path, and they are difficult to occur at room temperature without NTP.

In summary, reactions for the generation of main products in the experiment (SOF_2, SO_2F_2, SO_2) have different energy barriers. SOF_4 is generated relatively early, and it also acts as an intermediate to generate other products. The generation of SO_2 is more difficult than SO_2F_2 from the perspective of SO_2F, as it has the highest energy barrier in this degradation path. In addition, the generation of SO_2 requires SF_6 to leave six F atoms and combine with two O atoms, so its generation process is more complex than that of S-O-F gases. For SOF_2 and SO_2F_2, their generation processes undergo the decomposition of unstable intermediates with no obvious energy barriers.

From the point of view of surface reactions, γ-Al_2O_3 packing changes SF_6 decomposition in two main ways. First, γ-Al_2O_3 promotes the initial bond-breaking of SF_6. The activation barrier of SF_6^* to SF_5^* and F^* over the surface is 1.80 eV, which is much lower than the reaction heat in gas
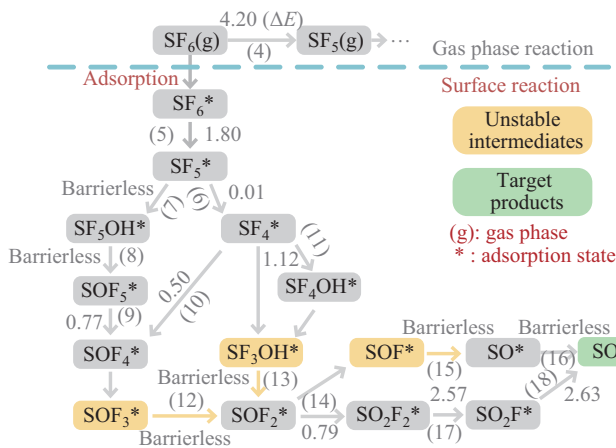
phase (4.20 eV). In this regard, SF$_6$ is much easier to undergo a stepwise decomposition over the packing surface. Second, active sites provided by packing material hold promise for adsorption and activation of SF$_6$ primary decompositions and intermediates by chemisorption, thus initiating and facilitating surface reactions with necessary adsorbates.

However, it should be noted generation reactions of these unstable intermediates are difficult to determine by NEB methods, which may have high energy barriers also. Therefore, actual barriers for generating SOF$_2$ and SO$_2$F$_2$ may also be high, and such investigations require more in-situ experimental details and more advanced calculation methods, which is beyond the scope of this paper.

In this part, we mainly focus on the generation of key products like S-O-F gases and SO$_2$, because they are the main stable products in NTP treatment, and S-O-F gases are target products to be reduced. Detached F from SF$_6$ could easily bond with H or O atoms to form HF and OF_2 or undergo self-bonding to form F_2 [10]. These fluorine gases are reactive and can be easily handled by the alkaline solution, which is not discussed in detail in this paper. It should be noted the whole degradation path of SF$_6$ should contain more intermediates and branches, while some of them may even play an important role in the degradation process. Therefore, it's worth further investigation when more detailed information on products in-situ and ex-situ is provided.

D. Effects of The Plasma Radicals

Previous studies have proven that additional H$_2$O and O$_2$, as well as SF$_6$ in DBD plasma, can produce a large number of radicals like H, O, OH, and F [16]. According to plasma-catalysis theory, high-energy radicals can move to the packing material surface and react with adsorbed species via the Eley-Rideal (ER) mechanism [41]. That is, active particles in gas phase do not undergo the adsorption process but react directly with pre-adsorbed surface species. By contrast, if there are no active particles, the reaction mainly happens among adsorbed species via Langmuir-Hinshelwood (LH) mechanism.

In this work, three typical radicals, i.e., O, H, and F are considered, and six ER reactions are calculated, as listed in Table III (21)–(26). ER reactions mainly focus on the generation of stable products and their promotional effect on gas decomposition. For better comparison, the energy path and change in key bond length of each ER reaction are summarized in contrast to their LH reactions, as shown in Fig. 6 to 8. Besides, reaction (24) has no LH reaction counterpart, and (25) and (26) reactions contrast themselves, as shown in Figs. 9 and 10.

Figure 6 shows comparison of SOF$_4$* formation between LH reaction (10) and ER reaction (20). It is easy to see there are obvious differences in distributions of energy path and O-S distance. SOF$_4$* formation via LH process has a reaction energy barrier of 0.50 eV, while its ER process is barrierless, and the energy path decreases all the way. During ER process, O radical with high energy first approaches the SF$_4$* molecule and then releases a large amount of energy when O-S distance is reduced to about 4 Å, as shown in coordinates 6–8 in Fig. 6(b), where 'g' means the molecule is initialed in
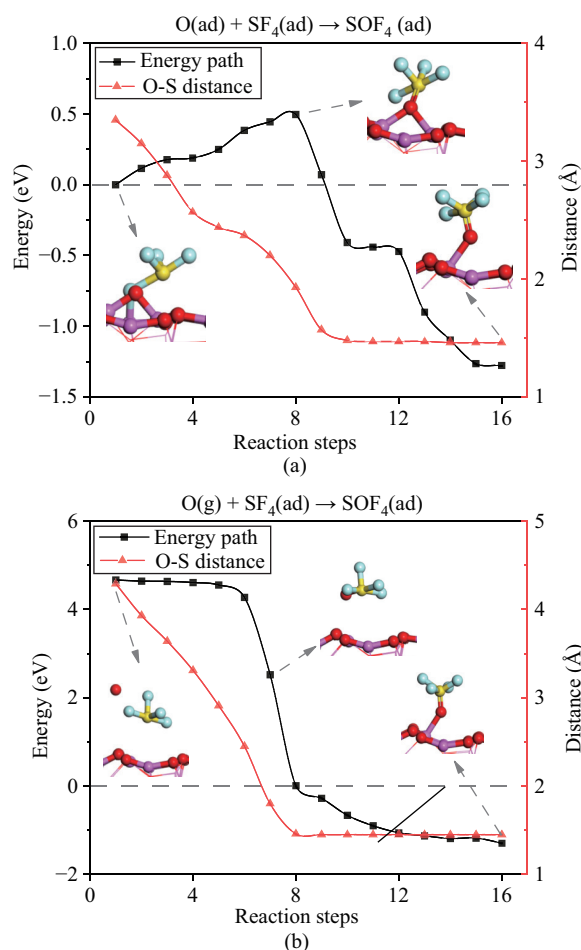
gas phase. Then O radical bonds with SF$_4$* to produce a stable SOF$_4$* over γ-Al$_2$O$_3$ (110) surface. Therefore, SOF$_4$ formation can be promoted by O radicals via ER reactions.

Formation of SO$_2$F$_2$ via LH reaction (15) and ER reaction (22) are shown in Fig. 7. In LH reaction, SOF$_2$* gradually bonds with O* on γ-Al$_2$O$_3$ surface, with an activation barrier of 0.79 eV. In Fig. 7(b), the O(g) radical moves from gas phase to γ-Al$_2$O$_3$ surface with S-O distance decreasing. Once S-O distance reaches about 2.0 Å, the O(g) undergoes a bonding process with rapid energy release. This ER reaction does not have an activation barrier either. In the plasma region, O radicals are mostly produced by O$_2$ dissociation, thus facilitating SO$_2$F$_2$ generation. This corresponds well with experimental results in Fig. 3 that increasing O$_2$ concentration significantly promotes SO$_2$F$_2$ yield.

In Fig. 8(a), SO$_2$F* decomposes to SO$_2$* and F* via reaction (19) with a high barrier of 2.63 eV. This may be due to stable S-F bonding in SO$_2$F, which needs high energy to activate. By contrast, in Fig. 8(b), H radicals can react with SO$_2$F* to form HF(g), then HF(g) decomposes to H* and F*. The whole reaction shows no obvious barrier, which means it is much easier to occur than the reaction (19). In a word, reactive radicals generated in the plasma region are likely to undergo a strong interaction process with surface intermediates, leading
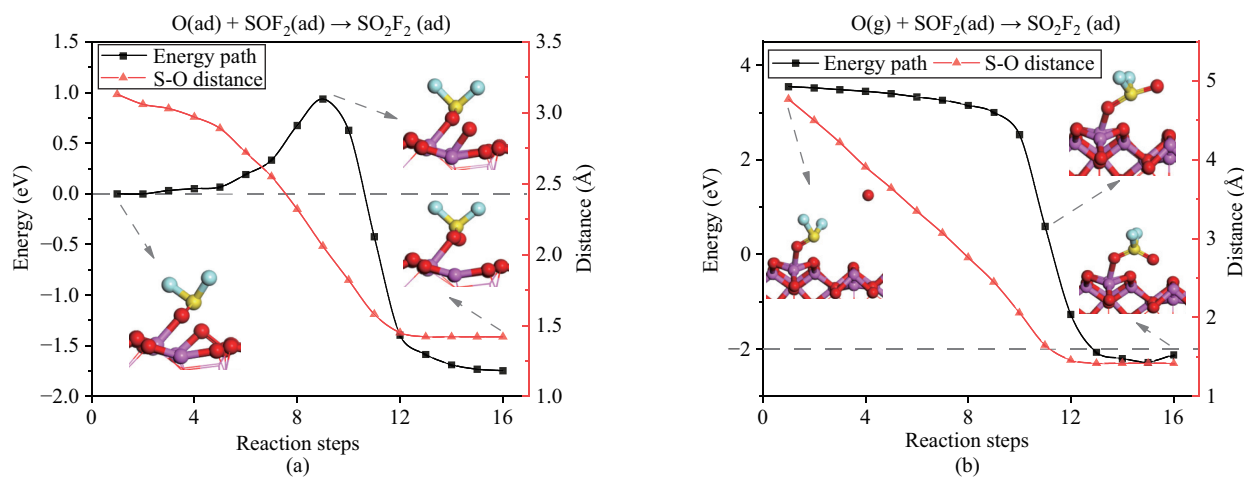

Fig. 6. Formation of SOF$_4$ by O and SF$_4$ via (a) LH reaction and (b) ER reaction. O(ad) and O(g) mean O atom is in the adsorbed state and the radical state, respectively.

Fig. 7. Formation of SO_2F_2 by O and SOF_2 via (a) LH reaction and (b) ER reaction. O(ad) and O(g) mean O atom is in the adsorbed state and the radical state, respectively.
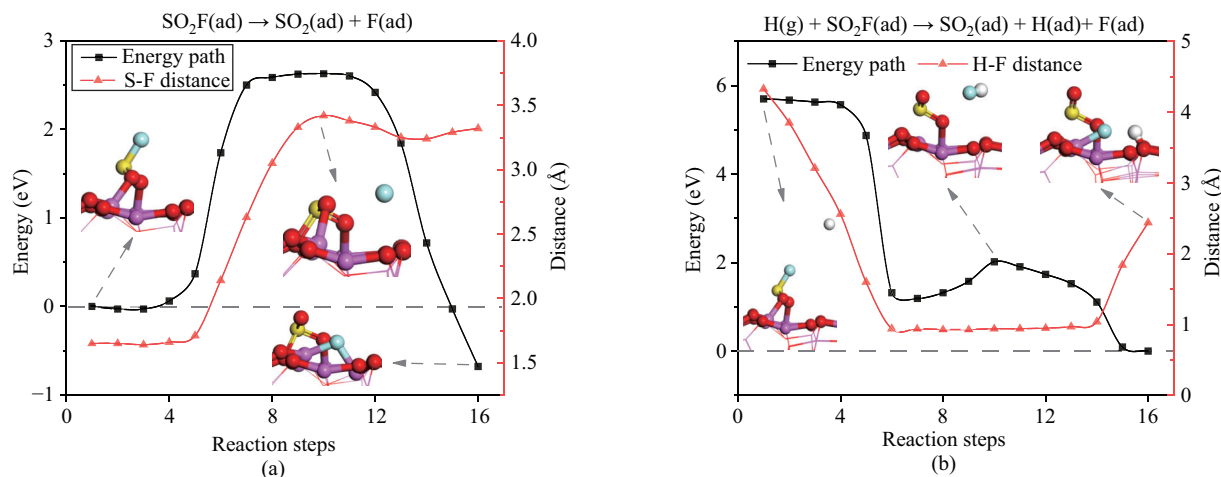

Fig. 8. Formation of SO_2 via (a) LH reaction and (b) ER reaction. H(g) means the H atom is in the radical state, respectively.

to further degradation of some products and accelerating the degradation reactions. Meanwhile, additional gases like NH_3 or H_2O in the plasma region can produce H(g) radicals, promoting the production of SO_2 by reactions like Fig. 7(b), thus affecting product selectivity. This corresponds well with the results in Fig. 3(a).

In Fig. 9, the decomposition of SOF_4 via ER reaction (24) is similar to Fig. 8(b). H radical can 'collide' with SOF_4* and bond with one F atom to form an HF(g), while SOF_4* loses one F atom to form a SOF_3* intermediate. Then SOF_3* can further decompose to SOF_2* and F*. Thus, with help of H radicals, SOF_4, as a relative stable intermediate, can have further decomposition to produce more stable products such as SOF_2. Moreover, the presence of H(g) corresponds to the addition of H-containing gases, like NH_3, H_2O and H_2. In Fig. 3(a), the selectivity of SOF_2 in the H_2O added system is obviously higher than O_2 added system, which may be caused by reaction (24).

Figure 10 shows the formation of HF(g) via ER reactions when H or F radicals are involved. It's easy to find H or F radicals in gas phase that can react with surface F* or H* species and form desorbed HF(g) molecules via reactions (25)
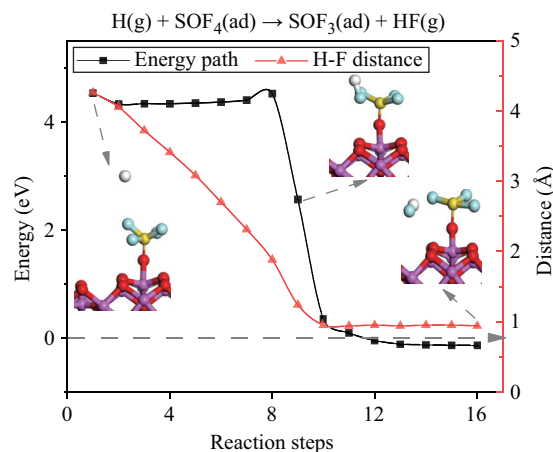

Fig. 9. Decomposition of SOF_4 via ER reaction.

and (26) without a barrier. By contrast, combination of H* and F* to HF* and its desorption has a barrier of 1.17 eV. This indicates in the presence of H-containing gases, H radicals can have ER reactions to generate HF(g). Similarly, increasing input power can promote the generation of F radicals, which
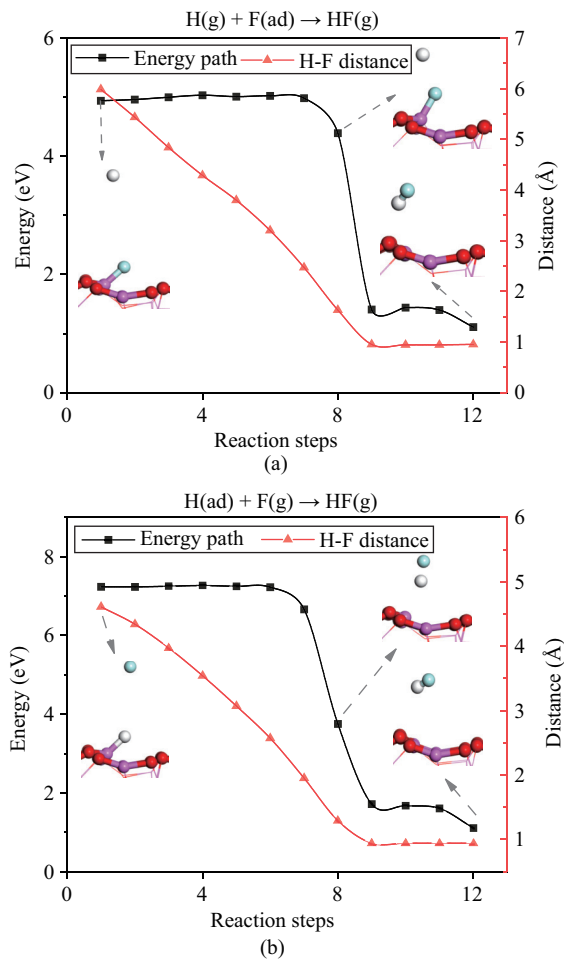
Fig. 10. Formation of HF by (a) H radical and adsorbed F and (b) adsorbed H and F radical via ER reactions.

is also expected to promote HF(g) yield. These two processes could take away the F element from packed bed system, resulting in lower selectivity of S-O-F gas products and promoting SO$_2$ yield.

Compared to non-packed DBD treatment in previous studies [30], γ-Al$_2$O$_3$ packing provides a gas-solid interface, which is better for discharge and degradation [12], [17], [27]. In the packed-bed system, reactive gases generate surface-adsorbed species and high-energy radicals during discharge. LH reactions occurring on the packing surface will drive SF$_6$ to start a significant reaction path dispersion after 1 or 2 F detachments. SOF$_4$ is a relatively stable product under insufficient degradation conditions [30], but it is further decomposed in packing systems, especially when radicals are involved, so it is basically not detected in this experiment (part per million level). SO$_2$ generation process has the highest reaction energy barrier with the most reactive processes and is, therefore, theoretically the most difficult to occur. However, our DFT calculations reveal that H radicals can promote SO$_2$ generation on γ-Al$_2$O$_3$ surface via ER reactions with no significant energy barrier. This corresponds well with the experimental promotion phenomenon of SO$_2$ by H$_2$O addition. Further, H radicals and H* can effectively combine with F radicals and F* at the gas-solid interface to form HF(g), which

can be carried away from the reactor, and this process could be one main reason for the reduction of S-O-F selectivity caused by H$_2$O addition. The type and content of free radicals will significantly affect the degradation efficiency and product generation path of SF$_6$.

It should be noted that the above-mentioned reactions are only a limited part of reactions involving O, H, and F radicals. Meanwhile, apart from the above three radicals, there are other radicals such as Ar, OH, Si, and N, all of which may participate in the degradation process via ER reactions. As we proposed, the above reactions are examples of elaborate effects of radicals in plasma on surface reactions and product regulation. In the future, in-situ information on gas-phase radicals and surface adsorbed species is vital for further investigation of SF$_6$ degradation mechanism in a plasma-catalytic system.

IV. CONCLUSION

Understanding SF$_6$ degradation mechanism in NTP system is important to determine harmless and effective abatement strategies. In this study, we conducted a detailed investigation of SF$_6$ degradation process and generation of main S-contained products by combining a discharge experiment and a DFT calculation for a γ-Al$_2$O$_3$ packed-bed DBD system. In the experiment, 0.25%–2.5% H$_2$O and 0.05%–4% O$_2$ are separately added in 3%SF$_6$-97%Ar mixture. The addition of H$_2$O or O$_2$ can improve SO$_2$ yield or SO$_2$F$_2$ yield, respectively, showing a regulation property on SF$_6$ products. Besides, the total yields of three stable products in this work reach a level of ∼40 nmol/J, which is much higher than in typical spark (∼2 nmol/J) or corona discharges (∼15 nmol/J), which proves the capability of PB-DBD on effective abatement of SF$_6$.

In DFT calculations, adsorption properties of 16 possible decompositions are tested over γ-Al$_2$O$_3$ (110) surface. SF$_5$, SF$_5$OH, SOF$_5$, SOF$_4$, SF$_4$OH, SOF$_2$ SO$_2$F$_2$, SO$_2$F and SO$_2$ can chemically adsorb at Al$_{III}$ surface site. SF$_4$ shows physical adsorption over Al$_{III}$ atom. S$_2$F$_{10}$, SF$_3$OH, SOF$_3$, SOF, and HF are not stable and undergo further decomposition. After that, 14 possible degradation reactions of SF$_6$ over the γ-Al$_2$O$_3$ (110) surface with H, OH, or O pre-adsorbed species are calculated via LH mechanism. Results show SF$_6$ could undergo different reactions with surface species when one or two F is detached, i.e., SF$_5$ or SF$_4$ are generated. SOF$_4$ could act as an intermediate in the degradation path to further produce SOF$_2$. SO$_2$ is the hardest to generate, with the highest activation barrier and most complicated reaction steps. The effect of plasma-generated radicals (H, O, and F) on surface reactions is studied via 6 possible ER reactions. High-energy radicals show high reactivity in surface reactions and effectively promote further decomposition of adsorbed species (such as SOF$_4$) or generation of some final products (SO$_2$, SO$_2$F$_2$, and HF), which correspond well with experimental product results.

In general, the degradation of SF$_6$ with reactive gases in packed-bed plasma is very complicated. Plasma-generated radicals from reactive gases are one important factor in determining surface reactions via ER mechanism, which leads to a deep decomposition of SF$_6$ and regulation of by-products.

REFERENCES

[1] G. Chen, Y. P. Tu, C. Wang, J. Wang, Z. K, Yuan, G. M. Ma, J. Wang, B. Qi, and C. Y. Li, "Environment-friendly insulating gases for HVDC gas-insulated transmission lines," *CSEE Journal of Power and Energy Systems*, vol. 7, no. 3, pp. 510–529, May 2021.

[2] J. R. Wang, Q. M. Li, H. Liu, J. Wang, Y. N. Chang, Q. Hu, and M. A. Haddad, "Impact of SF6 Decomposition Products on Epoxy Resin Chemical Stability and Doping-nano-Al$_2$O$_3$-based Enhancement Using the ReaxFF-MD Method," *CSEE Journal of Power and Energy Systems*, vol. 9, no. 2, pp. 779–789, Mar. 2023.

[3] X. K. Fang, X. Hu, G. Janssens-Maenhout, J. Wu, J. R. Han, S. S. Su, J. B. Zhang, and J. X. Hu, "Sulfur hexafluoride (SF$_6$) emission estimates for China: an inventory for 1990–2010 and a projection to 2020," *Environmental Science & Technology*, vol. 47, no. 8, pp. 3848–3855. Mar. 2013.

[4] M. Y. Zhao, D. Han, W. K. Zhao, Z. R. Zhou and G. Q. Zhang, "Experimental and Theoretical Studies of C$_3$F$_7$CN/CO$_2$ Mixture Decomposition Under Overheating Fault," *CSEE Journal of Power and Energy Systems*, vol. 8, no. 3, pp. 941–951, May 2022.

[5] X. X. Zhang, H. Y. Xiao, J. Tang, Z. L. Cui, and Y. Zhang, "Recent advances in decomposition of the most potent greenhouse gas SF$_6$," *Critical Reviews in Environmental Science and Technology*, vol. 47, no. 18, pp. 1763–1782, Dec. 2017.

[6] G. Zaccaro, J. M. Biasse, R. Coccioni, and P. Leoni, "State of the art process of end-of-life treatment for SF$_6$ medium voltage equipment," in *Eco-Design in Electrical Engineering*, J. L. Bessède, Ed. Cham: Springer, 2018, pp. 163–170.

[7] M. Shih, W. J. Lee, and C. Y. Chen, "Decomposition of SF$_6$ and H$_2$S mixture in radio frequency plasma environment," *Industrial & Engineering Chemistry Research*, vol. 42, no. 13, pp. 2906–2912, May 2003.

[8] A. Parthiban, A. A. R. Gopal, P. Siwayanan, and K. W. Chew, "Disposal methods, health effects and emission regulations for sulfur hexafluoride and its by-products," *Journal of Hazardous Materials*, vol. 417, pp. 126107, Sep. 2021.

[9] W. T. Tsai, "The decomposition products of sulfur hexafluoride (SF$_6$): reviews of environmental and health risk analysis," *Journal of Fluorine Chemistry*, vol. 128, no. 11, pp. 1345–1352, Nov. 2007.

[10] C. H. Tsai and J. M. Shao, "Formation of fluorine for abating sulfur hexafluoride in an atmospheric-pressure plasma environment," *Journal of Hazardous Materials*, vol. 157, no. 1, pp. 201–206, Aug. 2008.

[11] X. X. Zhang, Z. L. Cui, Y. L. Li, H. Y. Xiao, Y. Li, J. Tang, and S. Xiao, "Abatement of SF$_6$ in the presence of NH$_3$ by dielectric barrier discharge plasma," *Journal of Hazardous Materials*, vol. 360, pp. 341–348, Oct. 2018.

[12] Z. L. Cui, X. X. Zhang, Y. Tian, X. Y. Pan, Y. Luo, and J. Tang, "Plasma-assisted abatement of SF$_6$ in a dielectric barrier discharge reactor: investigation of the effect of packing materials," *Journal of Physics D: Applied Physics*, vol. 53, no. 2, pp. 025205, Jan. 2020.

[13] J. Tang, F. Liu, X. X. Zhang, Q. H. Meng, and J. B. Zhou, "Partial discharge recognition through an analysis of SF$_6$ decomposition products part 1: decomposition characteristics of SF$_6$ under four different partial discharges," *IEEE Transactions on Dielectrics and Electrical Insulation*, vol. 19, no. 1, pp. 29–36, Feb. 2012.

[14] Y. W. Fu, A. J. Yang, X. H. Wang, A. B. Murphy, X. Li, D. X. Liu, Y. Wu, and M. Z. Rong, "Theoretical study of the neutral decomposition of SF$_6$ in the presence of H$_2$O and O$_2$ in discharges in power equipment," *Journal of Physics D: Applied Physics*, vol. 49, no. 38, pp. 385203, Sep. 2016.

[15] L. P. Zhong, S. C. Ji, F. Wang, Q. Q. Sun, S. Chen, J. Liu, B. Hai, and L. Tang, "Theoretical study of the chemical decomposition mechanism and model of Sulfur hexafluorid (SF$_6$) under corona discharge," *Journal of Fluorine Chemistry*, vol. 220, pp. 61–68, Apr. 2019.

[16] H. Y. Xiao, X. X. Zhang, X. X. Hu, and Q. D. Zhu, "Experimental and simulation analysis on by-products of treatment of SF$_6$ using dielectric barrier discharge," *IEEE Transactions on Dielectrics and Electrical Insulation*, vol. 24, no. 3, pp. 1617–1624, Jun. 2017.

[17] Z. L. Cui, C. Zhou, A. Jafarzadeh, S. Y. Meng, Y. H. Yi, Y. F. Wang, X. X. Zhang, Y. P. Hao, L. C. Li, and A. Bogaerts, "SF$_6$ catalytic degradation in a γ-Al$_2$O$_3$ packed bed plasma system: a combined experimental and theoretical study," *High Voltage*, vol. 7, no. 6, pp. 1048–1058, Dec. 2022.

[18] J. Hutter, M. Iannuzzi, F. Schiffmann, and J. VandeVondele, "CP2K: atomistic simulations of condensed matter systems," *WIREs Computational Molecular Science*, vol. 4, no. 1, pp. 15–25, Jan./Feb 2014.

[19] J. VandeVondele and J. Hutter, "Gaussian basis sets for accurate calculations on molecular systems in gas and condensed phases," *The Journal of Chemical Physics*, vol. 127, no. 11, pp. 114105, Sep. 2007.

[20] J. P. Perdew, K. Burke, and M. Ernzerhof, "Generalized gradient approximation made simple," *Physical Review Letters*, vol. 77, no. 18, pp. 3865–3868, Oct. 1996.

[21] S. Grimme, J. Antony, S. Ehrlich, and H. Krieg, "A consistent and accurate *ab initio* parametrization of density functional dispersion correction (DFT-D) for the 94 elements H-Pu," *The Journal of Chemical Physics*, vol. 132, no. 15, pp. 154104, Apr. 2010.

[22] S. Goedecker, M. Teter, and J. Hutter, "Separable dual-space Gaussian pseudopotentials," *Physical Review B*, vol. 54, no. 3, pp. 1703–1710, Jul. 1996.

[23] J. D. Head and M. C. Zerner, "A Broyden—Fletcher—Goldfarb—Shanno optimization procedure for molecular geometries," *Chemical Physics Letters*, vol. 122, no. 3, pp. 264–270, Dec. 1985.

[24] G. Henkelman, B. P. Uberuaga, and H. Jónsson, "A climbing image nudged elastic band method for finding saddle points and minimum energy paths," *The Journal of Chemical Physics*, vol. 113, no. 22, pp. 9901–9904, Dec. 2000.

[25] M. Digne, P. Sautet, P. Raybaud, P. Euzen, and H. Toulhoat, "Use of DFT to achieve a rational understanding of acid–basic properties of γ-alumina surfaces," *Journal of Catalysis*, vol. 226, no. 1, pp. 54–68, Aug. 2004.

[26] K. M. Bal, S. Huygh, A. Bogaerts, and E. C. Neyts, "Effect of plasma-induced surface charging on catalytic processes: application to CO$_2$ activation," *Plasma Sources Science and Technology*, vol. 27, no. 2, pp. 024001, Feb. 2018.

[27] X. X. Zhang, Y. Tian, Z. L. Cui, and J. Tang, "Plasma-assisted abatement of SF$_6$ in a packed bed plasma reactor: understanding the effect of gas composition," *Plasma Science and Technology*, vol. 22, no. 5, pp. 055502, May 2020.

[28] Y. Tian, X. X. Zhang, B. W. Tang, Z. L. Cui, G. Z. Zhang, Z. W. Chen, and H. Wang, "SF$_6$ abatement in a packed bed plasma reactor: study towards the effect of O$_2$ concentration," *RSC Advances*, vol. 9, no. 60, pp. 34827–34836, Oct. 2019.

[29] H. M. Lee, M. B. Chang, and K. Y. Wu, "Abatement of sulfur hexafluoride emissions from the semiconductor manufacturing process by atmospheric-pressure plasmas," *Journal of the Air & Waste Management Association*, vol. 54, no. 8, pp. 960–970, Aug. 2004.

[30] X. X. Zhang, Z. L. Cui, Y. L. Li, H. Y. Xiao, Y. Li, and J. Tang, "Study on degradation of SF$_6$ in the presence of H$_2$O and O$_2$ using dielectric barrier discharge," *IEEE Access*, vol. 6, pp. 72748–72756, Nov. 2018.

[31] F. Y. Chu, "SF$_6$ decomposition in gas-insulated equipment," *IEEE Transactions on Electrical Insulation*, vol. EI-21, no. 5, pp. 693–725. Oct. 1986.

[32] L. G. Christophorou and M. O. Pace, "Gaseous Dielectrics IV: Proceedings of the Fourth International Symposium on Gaseous Dielectrics," Knoxville, Tennessee, U.S.A., April 29-May 3, 1984.

[33] J. P. Manion, J. A. Philosophos, and M. B. Robinson, "Arc stability of electronegative gases," *IEEE Transactions on Electrical Insulation*, vol. EI-2, no. 1, pp. 1–10, Apr. 1967.

[34] X. H. Wang, Q. Q. Gao, Y. W. Fu, A. J. Yang, M. Z. Rong, Y. Wu, C. P. Niu, and A. B. Murphy, "Dominant particles and reactions in a two-temperature chemical kinetic model of a decaying SF$_6$ arc," *Journal of Physics D: Applied Physics*, vol. 49, no. 10, pp. 105502, Mar. 2016.

[35] Y. P. Raizer and J. E. Allen, *Gas Discharge Physics*, Berlin: Springer, 1991.

[36] H. H. Kim, Y. Teramoto, and A. Ogata, "Plasma-catalyst interactions," in *Plasma Catalysis: Fundamentals and Applications*, X. Tu, J. C. Whitehead, and T. Nozaki, Eds. Cham: Springer, 2019, pp. 47–68.

[37] J. Tang, J. Y. Pan, Q. Yao, Y. L. Miao, X. J. Huang, and F. P. Zeng, "Feature extraction of SF$_6$ thermal decomposition characteristics to diagnose overheating fault," *IET Science, Measurement & Technology*, vol. 9, no. 6, pp. 751–757, Sep. 2015.

[38] J. Tang, F. Liu, Q. H. Meng, X. X. Zhang, and J. G. Tao, "Partial discharge recognition through an analysis of SF$_6$ decomposition products part 2: feature extraction and decision tree-based pattern recognition,"

IEEE Transactions on Dielectrics and Electrical Insulation, vol. 19, no. 1, pp. 37–44, Feb. 2012.

[39] M. W. Chase, *NIST-JANAF Thermochemical Tables*, 4th ed., Woodbury: American Institute of Physics for the National Institute of Standards and Technology, 1998.

[40] Y. W. Fu, M. Z. Rong, K. Yang, A. J. Yang, X. H. Wang, Q. Q. Gao, D. X. Liu, and A. B. Murphy, "Calculated rate constants of the chemical reactions involving the main byproducts SO$_2$F, SOF$_2$, SO$_2$F$_2$ of SF$_6$ decomposition in power equipment," *Journal of Physics D: Applied Physics*, vol. 49, no. 15, pp. 155502, Apr. 2016.

[41] E. C. Neyts, K. Ostrikov, M. K. Sunkara, and A. Bogaerts, "Plasma catalysis: synergistic effects at the nanoscale," *Chemical Reviews*, vol. 115, no. 24, pp. 13408–13446, Nov. 2015.

Xiaoxing Zhang received B.S. and M.S degrees from Hubei University of Technology, and the Ph.D. degree from Chongqing University. He is currently a Professor at School of Electrical and Electronic Engineering, Hubei University of Technology. His research focuses on the online monitoring and fault diagnosis of high-voltage electrical insulation equipment, eco-friendly gas insulating medium and intelligence power sensors.

Peng Gao received his B.S. degree from Hubei University of Technology and now is a master's student here. His research interests include SF$_6$ degradation technology, surface adsorption and microcosmic modelling.

Zhaolun Cui obtained B.S. and Ph.D. degrees from Wuhan University in 2016 and 2021, respectively. He is now with South China University of Technology, as an Assistant Researcher Fellow. His current research interests are plasma-assisted treatment of greenhouse gas and online monitoring of high-voltage electrical insulation equipment.

Licheng Li received the B.S. degree from Tsinghua University, China, in 1967. He is a Member of the Chinese Academy of Engineering (CAE) and a Professor and Doctoral Supervisor at the South China University of Technology. His primary research fields include HVAC/HVDC transmission networks, paralleling system operation and stability, and wide-area measurement and control.

Chang Zhou received B.S. and M.S degrees from Hubei University of Technology. He is currently an Engineer in State Grid Xianning Electric Power Supply Company. His research focuses on the plasma-assisted SF$_6$ abatement.

Yanpeng Hao received B.S. and Ph.D. degrees from Xi'an Jiaotong University, China, in 1998 and 2003, respectively. She is now a Professor at South China University of Technology, China. Her major research field is insulation condition monitoring of electrical equipment.

Amin Jafarzadeh received his Ph.D. degree in Computational Chemistry from the University of Antwerp in 2020. Following this, he contributed as a postdoctoral researcher at the Catalysis Center for Energy Innovation, affiliated with the University of Delaware. Presently, he serves as a Guest Researcher at the University of Antwerp, while also holding the role of R&D Manager within the chemical industry.